LARGE EDDY SIMULATION OF SHOCK/BOUNDARY LAYER INTERACTION

E. GARNIER AND P. SAGAUT
ONERA
29, Av. de la Division Leclerc, BP72, 92322 Châtillon Cedex, FRANCE

AND

M. DEVILLE
Laboratoire de Mécanique des Fluides
Ecole Polytechnique Fédérale de Lausanne, CH-1015 Lausanne SWITZERLAND

1. Introduction

Shock/Boundary layer interaction is still an important problem for supersonic aircraft designers. Such phenomena play an important role both for internal and external aerodynamic. These interactions can lead to an increase of drag, separation, loss of performances. Moreover, unsteadiness of the shock produces strong constrains on the structure, noise and modifies local heat transfer.

Since, for such interactions, results obtained with the RANS approach are not satisfactory [12], it appears natural to assess the capacity of LES to simulate such interaction. From a numerical point of view, it necessitates the use of schemes designed to minimize the numerical dissipation in shock-free region of the flow since it was demonstrated in [1] that the numerical dissipation of high-order shock-capturing scheme can exceed the subgrid-scale dissipation. To satisfy this requirement, we use a strategy [2] built on the mixing of the characteristic based filters [3] and a sensor [4] able to distinguish a turbulent fluctuation from a shock. To validate this approach, the case of the interaction of an oblique shock with a boundary layer developing on a plane plate was chosen since it has been extensively studied experimentally at IRPHE [6] [7].

2. Mathematical model

In this study, we have used the system of filtered Navier-Stokes equations proposed by Vreman [8]. Some terms are neglected as in [5]. The subgrid-scale model is the selective mixed scale model proposed by Sagaut [9]. This model was proven to behave particularly well for wall-bounded flow.

The numerical scheme is based on non-linear WENO filters defined in Ref. [2]. Let U^n denote the vector of the conservative variables evaluated at the time $n\Delta t$ and Δt be the time step, $\widehat{U}^{(n+1)}$ the vector of the conservative variables after the application of any explicit time integration scheme. This vector is spatially filtered to give the final state U^{n+1} ($U^{n+1} = \mathcal{F}(\widehat{U}^{(n+1)})$). The main point is that the time advancement is performed with a non-dissipative spatial operator (noted L). The filtering pass is decomposed as follows:

$$U^{(n+1)} = \mathcal{F}(\widehat{U}^{(n+1)}) = (I_d + \beta \Delta t L_f)(\widehat{U}^{(n+1)}) \tag{1}$$

where L_f is any dissipative operator, I_d is the identity and the switch β is defined as:

$$\begin{cases} \beta = 0 & \text{if } \Psi < \epsilon \\ \beta = 1 & \text{if } \Psi \geq \epsilon \end{cases} \tag{2}$$

where Ψ is the sensor of Ducros *et al.*[4] defined as:

$$\Psi = \frac{(div(\mathbf{u}))^2}{(div(\mathbf{u}))^2 + (rot(\mathbf{u}))^2} \tag{3}$$

where $\mathbf{u}$ denotes the velocity vector. This sensor was demonstrated to be able to distinguish a turbulent fluctuation from a shock in Refs. [4] and [2].

In this study, the time integration is performed by means of a third-order accurate TVD Runge-Kutta method proposed by Shu and Osher [10]: Note that L is referred to as "base scheme" and can be any qth order accurate finite volume or finite difference non-dissipative scheme.

As mentioned by Yee *et al.* [3], L_f can be the dissipative part of any shock-capturing scheme. Here, such operator is derived of ENO schemes. The dissipative part of ENO scheme is extracted easily by subtracting a centered scheme to the ENO one.

In this study, we have used a combination of a fourth-order centered base scheme with a fifth-order accurate WENO filter. The threshold ϵ is fixed to 0.04. In practice, this method limits the computation of the filter to about 20 percents of the total number of grid points.

Viscous fluxes are discretized by means of a second order accurate centered scheme. The CFL number is fixed to 0.5.

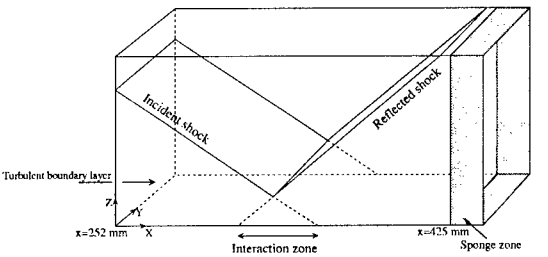

Figure 1. Computational domain

3. Description of the configuration

The shock is generated by a corner fixed to the upper plate of the wind tunnel and interacts with the turbulent boundary layer which develops on the lower plate (which is assumed to be adiabatic).

The length of the computational domain was restricted to the measurement zone (it begins at $x = 252\ mm$ and ends at $x = 440\ mm$). The height of the domain is $70,7\ mm$ whereas the height of the wind tunnel is $120\ mm$. The computational domain is presented in Fig. 1 (note that the axe x denotes the longitudinal direction, y the spanwise direction and z the wall-normal direction). The width of the computational domain is about $15\ mm$ in the spanwise direction (for the test cases A, C and D) whereas the wind tunnel is 10 times larger.

At the inflow (at $x = 252\ mm$), the temperature T_e outside of the boundary layer is $144.6\ K$, the density is equal to $9.66\ 10^{-2}\ kg/m^3$ and the Mach number is fixed to 2.3. The Reynolds number Re based on the displacement length $\delta_1 = 3.535\ mm$ is equal to 19132. Periodic boundary conditions are applied in the spanwise direction y. Non reflective conditions are applied on the upper frontier. At the outflow, a $13\ mm$ long sponge zone ensures the damping of turbulent fluctuations which are evacuated by means of non-reflective conditions. No-slip and adiabaticity conditions are applied on the wall.

In this study, four simulations have been carried out in order to check the sensitivity of the results to computational details. The characteristics of these simulations are reported in Table 1. The number of grid points (N_x, N_y, N_z) in each direction are mentioned and the size of the computational meshes (Δ_x^+, Δ_y^+, Δ_z^+) are given in wall units. We precise that these wall units are based on a experimentally measured friction velocity of $24.75 m/s$ at $x = 260\ mm$. Test case A is the base case. In test case B, the influence of a doubling of the domain size in the spanwise direction is investigated. The effect of a refined grid in the longitudinal direction is studied using case C and case D is devoted to the investigation of the importance of a

	N_x	N_y	N_z	Δ_x^+	Δ_y^+	$\Delta_z^+(min)$	SGS Model
Case A	255	55	151	50	18	1	*yes*
Case B	255	110	151	50	18	1	*yes*
Case C	510	55	151	25	18	1	*yes*
Case D	255	55	151	50	18	1	*no*

SGS model.

The generation of realistic inflow conditions is a very important issue in LES. In this study, we follow the methodology introduced by Lund *et al.* [11] and extended to compressible flow by Urbin *et al.*[13]. This strategy prevents the thickening of the boundary layer using an *ad hoc* re-scaling. The loss of self-similarity induced by the shock requires the Lund procedure to be applied on a second simulation of time-developing canonical turbulent boundary layer. A $x = cste$ plane of this second simulation is extracted and introduced in the shock/turbulence LES inflow plane at each time step.

4. Analysis of the results

First, iso-values of the mean pressure are presented in Fig. 2. The incident shock (which would impact near $x = 336\ mm$ in absence of boundary layer) curves penetrating the boundary layer (thick of 11 mm at the inflow) and reflects on the sonic line (also represented on the picture) as an expansion fan. The compression related to the rising of pressure waves in the subsonic part of the boundary layer focuses to form a reflected shock (whom the trace begins in the vicinity of the position $x = 290\ mm$ at the wall). The continuation of this shock would impact on the wall near $x = 275\ mm$ and marks the beginning of the interaction zone.

Iso-values of longitudinal velocity fluctuations are shown in Fig. 3. Upstream the interaction, these fluctuations are strong in the near wall region. One can observe that the fluctuations are amplified by a factor two under the reflected shock (near $x = 290\ mm$). The explanation given by Laurent [7] to explain this amplification of the fluctuations is a linear effect by rapid distorsion. The zone concerned by a high level of fluctuation spreads above the separated zone (near $x = 320\ mm$). In agreement with experimental observations, one can notice an alignment of the isovalue lines of the fluctuations with the reflected shock just downstream of this one. Downstream of the interaction zone, longitudinal and vertical (not shown) fluctuations are maximum in the middle of the boundary layer ($z/\delta \sim 0,6$). However, one can observe a second extremum of longitudinal fluctuations in the near wall region close to the outflow, this an evidence of a (slow) return toward an equilibrium state. A particular attention must be paid to the interpre-

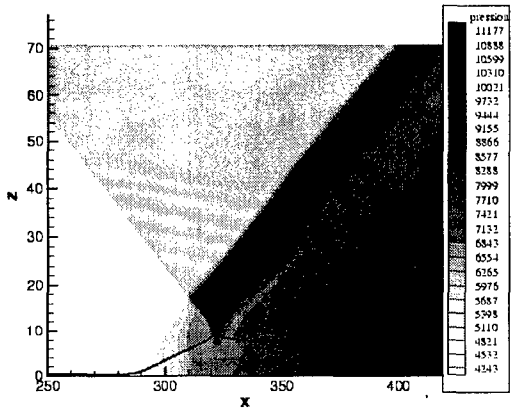

Figure 2. Iso-values of the mean pressure and sonic line (in black)

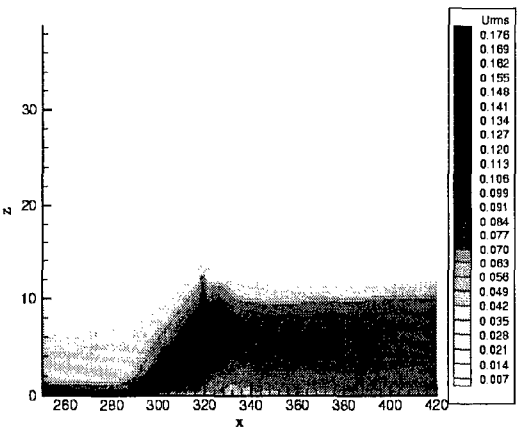

Figure 3. Iso-values of the mean longitudinal velocity fluctuations

tation of data concerning the fluctuations in the interaction zone since the unsteadiness of the shocks and of the recirculation bubble can be at the origin of a part of the fluctuations (it is then not possible to consider turbulent fluctuations).

Longitudinal evolution of the displacement thickness is displayed in Fig. 4. The computation of this integral quantity is not trivial since the external velocity $U_e(x)$ varies in the longitudinal direction. The potential flow is supposed to be reached when the Ducros sensor value exceeds 0.1.

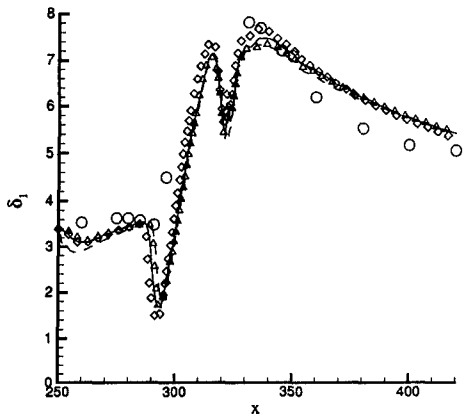

Figure 4. Longitudinal evolution of the displacement thickness
Case A ———, Case B △, Case C - - - - -, Case D ◇, HWA ○

This method gives results coherent with measurement since the value of δ_1 at the inflow of the computational domain is correctly predicted (at $x = 260\ mm$) after a short transient. The evolution of δ_1 in the interaction zone ($290\ mm < x < 340\ mm$) will not be commented in absence of corresponding experimental data. Looking at figure 4, one can observe that the displacement thickness is multiplied by a ratio larger than two during the interaction. This amplification rate is well predicted by computations and during the relaxation phase where δ_1 decreases, the discrepancies do not exceed 10 %.

The longitudinal evolution of the friction coefficient C_f is presented in Fig. 5 for the four cases and compared with Hot Wire Anemometry (HWA) data [7]. At the inflow, the discrepancies on the C_f between computations and experience is lower than 10 % for cases A and B. (such kind of underestimation is classical with LES [14]). Cases C (with the best resolution) and D give levels of C_f very close to the experiment. The flow is seen to be separated for cases A, B and C between $x = 290\ mm$ and $x = 340\ mm$. The quasi totality of the interaction zone is concerned by the separation. For the case D (without SGS model), the velocity fluctuations in the near wall zone are stronger and the flow separates latter (near $x = 305\ mm$). Just after the interaction zone ($x = 340\ mm$), experimental evaluations based on hypothesis of the existence of a logarithmic zone lead to a friction coefficient clearly positive at the opposite of the computations. In the relaxation zone, the increase of C_f between computations and experiment is very similar and, at the outflow, the discrepancies are comparable to those

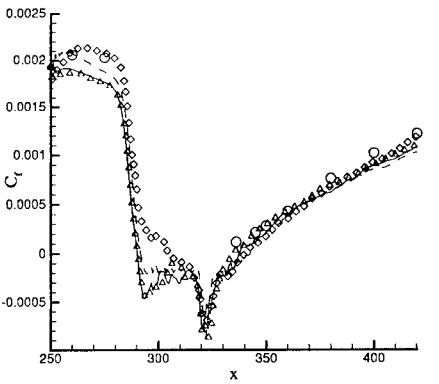

Figure 5. Longitudinal evolution of friction coefficient
Case A ———, Case B △, Case C - - - - -, Case D ◇, HWA ○

observed at the inflow (about 10 %). The results quality is clearly superior to the one obtained with RANS computations (see [12]) in the same configuration (but at $Ma = 2.9$).

Independently of the analysis of the results concerning physical variables, we verify in Fig. 6 that the Ducros sensor applies nearly exclusively in the zone where we have noticed in Fig. 2 the presence of shock or expansion. Consequently, the SGS model is effective (his effect is not masked by numerical dissipation) in the most part of the boundary layer. Nevertheless, one can observe low values of the sensor on the upper limit of the boundary layer where the adaptation of the inflow conditions may not be perfect. Even if this strategy of minimization of the numerical dissipation would merit other validation (see also [2]) on different test cases, results presented here allows to be confident with this concept.

5. Conclusion

Bidimensional interaction an oblique shock with a plane plate has been studied numerically using LES and compared with experimental data. Numerical results are in quantitative agreement with experimental results and LES can now be considered as a predictive tool for such physically complex flow. The separated zone is correctly described. The effects of the size of the domain in the spanwise direction, of the resolution in the longitudinal direction and the presence of a SGS model do not appear to be deciding.

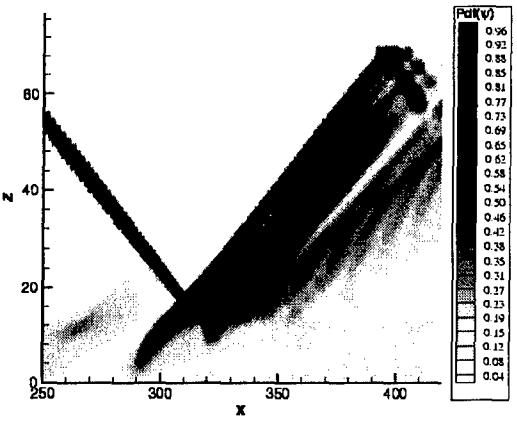

Figure 6. Iso-values of the mean PDF of Ducros sensor

References

1. E. Garnier, M. Mossi, P. Sagaut, P. Comte and M. Deville. On the use of shock-capturing scheme for Large-Eddy Simulation, *J. Comput. Phys.*, **153**, 273-311, 1999
2. E. Garnier, P. Sagaut and M. Deville. A class of explicit ENO filters with applications to unsteady flows, *J. Comput. Phys.*, **170**, 184-204, 2001
3. Yee, H. C., Sandham, N. D., and Djomehri, M. J., "Low-dissipative High-Order Shock-Capturing Methods Using Characteristic-Based Filters," *J. Comput. Phys.*, **150**, 199-238, 1999
4. F. Ducros, V. Ferrand, F. Nicoud, C. Weber, D. Darracq, C. Gacherieu and T. Poinsot. Large-Eddy Simulation of shock/turbulence interaction, *J. Comput. Phys.*, **152**, 517-549, 1999
5. Garnier, E., Sagaut, P., and Deville, M., "Large-Eddy Simulation of shock / homogeneous turbulence interaction," to be published in *Computers & Fluids*
6. J. Deleuze. Structure d'une couche limite turbulente soumise à une onde de choc incidente, *Thèse de doctorat, Université Aix-Marseille II*, 1995
7. H. Laurent. Turbulence d'une interaction onde de choc / couche limite sur une paroi adiabatique ou chauffée, *Thèse de Doctorat, Université Aix-Marseille II*, 1996
8. Vreman, B., Geurts, B., and Kuerten, H., "A priori tests of large eddy simulation of the compressible plane mixing layer," *Journal of Engineering Mathematics*, **29**, 299-327, 1995
9. Sagaut, P., "Large Eddy Simulation for incompressible flows," *Springer*, 2001
10. Shu, C. W., and Osher, S., "Efficient implementation of Essentially Non-Oscillatory shock-capturing schemes II," *J. Comput. Phys.*, **83**, 32-78, 1989
11. T. S. Lund, X. Wu and K. D. Squires. Generation of Turbulent Inflow Data for Spatially-Developing Boundary Layer Simulations. *J. Comput. Phys*, **140**, 233-258, 1998
12. D. P. Rizzetta. Evaluation of explicit Algebraic Reynolds-Stress Models for Separated Supersonic Flows, *AIAA J.*, **36**, 24-30, 1998
13. G. Urbin and D. Knight, Large Eddy Simulation of a Supersonic Boundary Layer Using an Unstructured Grid, *AIAA J.*, **39**, 1288-1295, 2001
14. E. T. Spyropoulos and G. A. Blaisdell. Large-Eddy Simulation of a spatially Evolving Supersonic Turbulent Boundary-Layer Flow, *AIAA J.*, **32**, 1983-1990, 1998